Springer

KSME

Journal of Mechanical Science and Technology 27 (6) (2013) 1693~1699
www.springerlink.com/content/1738-494x
DOI 10.1007/s12206-013-0418-y

Numerical study of droplet breakup and merging in a microfluidic channel †

Jaewon Lee, Woorim Lee and Gihun Son*

Department of Mechanical Engineering, Sogang University, Shinsu-dong, Mapo-gu, Seoul, 121-742, Korea

(Manuscript Received November 23, 2012; Revised February 27, 2013; Accepted March 4, 2013)

Abstract

Droplet breakup and merging in a microfluidic channel, which are applied to lab-on-a-chip devices for biomedical testing and synthesis, are simulated numerically by solving the conservation equations of mass and momentum. The droplet surface is computed using the volume-of-fluid method of the commercial code FLUENT. The numerical simulation demonstrates that the variation of obstacle geometry in a microchannel determines the droplet breakup pattern and the volume fraction of split droplets. The computation also shows that droplet merging depends on the channel-chamber width ratio. The effect of microchannel and obstacle configuration on the droplet motion is investigated to find the optimal conditions for droplet breakup and merging.

Keywords: Droplet breakup; Droplet merging; VOF (volume-of-fluid) method; Microfluidic channel

1. Introduction

Droplet breakup and merging in a microchannel are integral processes occurring in lab-on-a-chip (LOC) applications [1]. The droplet breakup into two or more pieces is required for parallel operations in bio experiments [2]. The droplet-droplet merging process is employed for chemical reaction and biomolecular synthesis [3, 4]. The present study focuses on accurate prediction and precise control of the droplet motions, which are very important for efficient LOC applications.

Droplet breakup was achieved by Song et al. [5] using a T-junction channel. The variation of the flow rates in the branching channels was observed to precisely control the size of the split droplets. Link et al. [6] proposed another method placing a single obstacle in a microfluidic channel. This method could significantly reduce the device space compared with the T-junction method. However, the use of an obstacle required the addition of a surfactant to prevent the coalescence of split droplets and was less reliable for precise control of the size of the split droplets than the T-junction method.

Droplet merging in a microchannel was obtained by Liu et al. [7] and Tan et al. [8] adding a chamber larger than the droplet diameter, which delayed the leading droplet to be merged with the following droplet. The widened channel geometry provided sufficient time to merge two droplets. Kohler et al. [9] added a widening channel to stop and trap the leading droplet in a droplet merging experiment. Chokkalingam et al. [10] proposed a different type of technique using a narrow channel part to delay the leading droplet. Droplet merging was usually achieved using a chamber or widening channel. However, these droplet merging methods also had a large space.

Recently, numerical analysis was performed to figure out the droplet breakup process and optimize the geometry configuration for the process. Droplet breakup in a T-junction channel was computed by De Menech [11] using a phase-field method, in which the droplet surface was determined by the molar fraction of a particular phase that was coupled to the free energy function. Carlson et al. [12] extended the phase-field method to simulation of droplet motion in a Y-junction channel. Their results showed that the tip of the junction affected the droplet deformation, and the droplet breakup or non-breakup regime depended on the capillary number and droplet size. The droplet breakup by a circular cylinder in a microchannel was computed by Chung et al. [13] using a front tracking method, in which the droplet shape was represented by the moving front elements. Their numerical results showed that the split droplets merged in the rear side of the obstacle when the capillary number was not large.

Few computations were made for droplet merging in a microchannel. Kadoura [14] applied the volume-of-fluid (VOF) method of the commercial code FLUENT to the droplet merging process using the electrowetting technique, which changed the contact angle. However, the variation of the channel geometry, which was a popular technique for droplet merging, was not investigated numerically.

*Corresponding author. Tel.: +82 2 705 8641, Fax.: +82 2 712 0799
E-mail address: gihun@sogang.ac.kr
† This paper was presented at the ISFMFE 2012, Jeju, Korea, October 2012. Recommended by Guest Editor Hyung Hee Cho

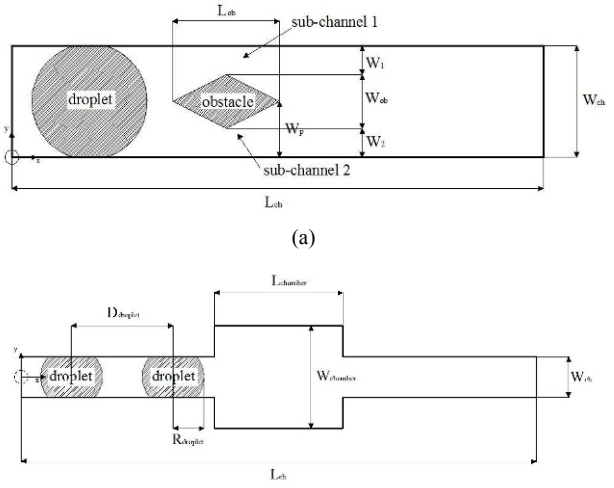

(a)

(b)

Fig. 1. Configuration used for simulation of droplet deformation in a microchannel: (a) droplet breakup; (b) droplet merging.

In this study, numerical simulations of droplet breakup by the use of an obstacle and droplet merging by the use of a chamber in a microchannel are performed. Various obstacle and chamber configurations are tested to find the optimal conditions for droplet breakup and merging in a microchannel.

2. Numerical analysis

The present numerical method is based on the VOF method of the commercial code FLUENT. Fig. 1 shows the computational domain used for simulation of droplet breakup and merging in a microchannel. The flows are taken to be two-dimensional and laminar. The fluid density and viscosity are assumed to be constant in each phase.

The VOF method tracks the droplet surface using the volume fraction of each fluid throughout the domain. The subscript 1 is chosen for the continuous liquid (primary) phase, while the subscript 2 for the discrete liquid (droplet) phase. The movement of the interface is described from the distribution of α_1 and α_2 in a computational cell. The primary-secondary phase interface exists in the cells where α_1 lies between 0 and 1. In the VOF method, the conservation equation of mass and momentum for the two phases can be written as a single set of the following equations:

$$\nabla \cdot \mathbf{u} = 0 , \tag{1}$$

$$\frac{\partial(\rho \mathbf{u})}{\partial t} + \nabla \cdot (\rho \mathbf{u}\mathbf{u}) = -\nabla p + \nabla \cdot \left[\mu(\nabla \mathbf{u} + \nabla \mathbf{u}^T)\right] + \mathbf{F}_{sur} \tag{2}$$

where

$$\rho = \alpha_1 \rho_1 + (1-\alpha_1)\rho_2 \tag{3}$$

$$\mu = \alpha_1 \mu_1 + (1-\alpha_1)\mu_2 \tag{4}$$

$$\boldsymbol{F}_{sur} = \sigma \frac{2\rho\kappa_1 \nabla \alpha_1}{\rho_1 + \rho_2} . \tag{5}$$

Here, the surface tension force $\mathbf{F}_{sur}$ in the momentum equation is expressed as a body force term which is localized near the fluid-fluid interface. The interface curvature κ is computed as

$$\kappa_1 = -\nabla \cdot (\nabla \alpha_1 / |\nabla \alpha_1|) . \tag{6}$$

The surface tension term reflects the interfacial force between the discrete liquid (droplet) and the continuous liquid. The interaction (attraction or repulsion) between droplets results from the continuous liquid flow which is affected by the interfacial forces existing at each droplet surface.

The droplet surface is tracked by solving the advection equation for the volume fraction of the secondary phase, which is written as

$$\frac{\partial}{\partial t}\alpha_2 + \nabla \cdot (\alpha_2 \mathbf{u}) = 0 . \tag{7}$$

The primary-phase volume fraction is computed by

$$\alpha_1 = 1 - \alpha_2 . \tag{8}$$

The boundary conditions used in this study are as follows (refer to Fig. 1).
At the inlet ($x = 0$),

$$u = u_{in} , \quad v = 0 . \tag{9}$$

At the outlet ($x = L_{ch}$),

$$P = P_{atm} . \tag{10}$$

At the walls ($y = 0, W_{ch}$),

$$u = u_{in} , \quad v = 0 , \quad \theta = 175^\circ . \tag{11}$$

The second-order upwind scheme is used for discretization of the momentum equation. The PISO scheme is taken as the pressure-velocity coupling scheme, while the PRESTO! is taken as the pressure discretization scheme. The geometric reconstruction scheme is used for interpolation of the interface geometry.

3. Results and discussion

Numerical simulations of droplet breakup and merging are performed using the hexadecane properties for the droplet and the water properties for the continuous phase:

$$\mu_c = 1.0 \times 10^{-3} Pas , \quad \rho_c = 1.0 \times 10^3 kg/m^3 ,$$
$$\mu_d = 8.0 \times 10^{-3} Pas , \quad \rho_d = 7.69 \times 10^2 kg/m^3 ,$$
$$\sigma = 3.5 \times 10^{-2} N/m .$$

The computational domain is chosen as a rectangular channel, including an obstacle in the droplet breakup case and an

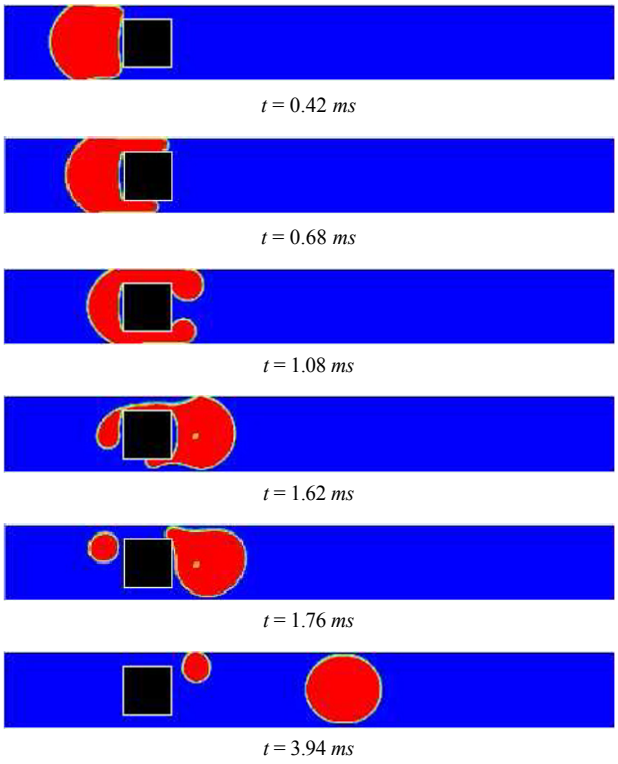

Fig. 2. Droplet breakup by a quadrate obstacle of $W_{ob} = L_{ob} = 0.63\,W_{ch}$, $W_1 = 0.2\,W_{ch}$ and $W_2 = 0.17\,W_{ch}$.

enlarged chamber in the droplet merging case, as depicted in Fig. 1.

A convergence test for grid resolutions is first conducted for droplet breakup by the use of a quadrate obstacle. When three different grid spacings of h = 2 μm, h = 1 μm and h = 0.5 μm are used, the computed fractional volumes of the broken primary droplets are 81%, 87%, and 88%, respectively. The relative difference of droplet volumes and interface shapes between successive mesh sizes is observed to be small as the mesh size decreases. Therefore, most the computations in this study are done with h = 1 μm to save computing time without losing the accuracy of the numerical results.

3.1 Droplet breakup

We varied the geometric configuration while keeping the channel width as $W_{ch} = 0.1$ mm, the inlet velocity as $u_{in} = 0.1$ m/s, and the initial droplet diameter as $1.1\,W_{ch}$. Due to the existence of obstacle, two sub-channels (or obstacle-channel gaps) are formed: sub-channel 1 near $y = W_{ch}$ and sub-channel 2 near $y = 0$. Initially, a droplet is placed at $x = W_{ch}$ from the channel inlet.

Fig. 2 shows the droplet breakup by a quadrate obstacle of $W_{ob} = L_{ob} = 0.63\,W_{ch}$, which is located at $W_1 = 0.2\,W_{ch}$ and $W_2 = 0.17\,W_{ch}$. When the droplet collides with the obstacle, it splits into the obstacle-wall gaps. As the droplet ends leave out

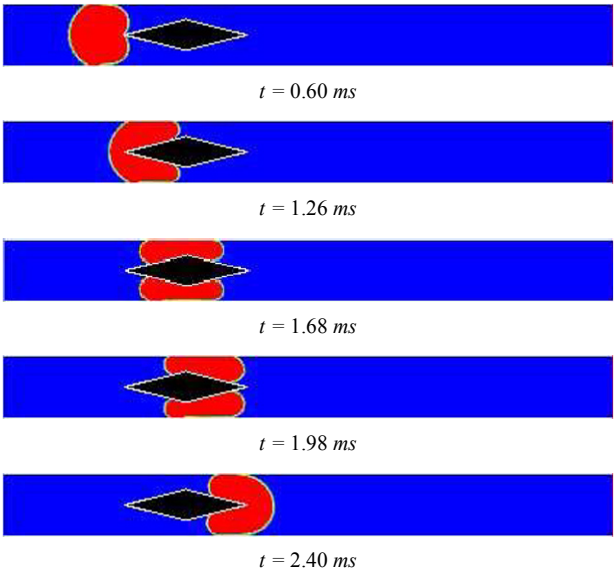

Fig. 3. Droplet breakup by a diamond-shape obstacle of $W_p = 0.5\,W_{ch}$.

of the gap, the droplet breakup occurs at a corner of the obstacle. The elongated droplet breaks off near the front and the rear corners of the quadrate obstacle. A broken small portion moves through the wider gap but does not merge with the main droplet. The broken small portion of droplet is not desirable for precise control of droplet. Since the size of the broken portion is related to the obstacle width, we introduce a diamond-shaped obstacle depicted in Fig. 1(a). When a diamond-shaped obstacle of $W_{ob} = 0.5\,W_{ch}$ and $L_{ob} = 2\,W_{ch}$, whose center is located at $x = 3\,W_{ch}$ and $y = 0.5\,W_{ch}$, is used, the droplet breakup occurs as Fig. 3, without any broken portion. In this case ($W_p = 0.5\,W_{ch}$), the split droplets re-merge. The droplet breakup pattern depends on the obstacle configuration. We vary W_p to find the obstacle configuration for droplet breakup without re-merging.

Fig. 4 shows the droplet merging for $W_p = 0.6\,W_{ch}$. Based on the steady - state velocity field without including a droplet, as presented in Fig. 5, the higher velocity is in the broad channel (sub - channel 2) than in the narrow channel (sub - channel 1) and the volume flow rate Q_2 in the sub-channel 2 is 54%. When the droplet enters the sub-channel, its interfaces move with different velocity, as seen at t = 1.20 *ms*. Then, the droplet is separated in the sub-channel, and the volume V_2 of the droplet in the sub-channel 2 is 53%, which is close to the volume flow rate ratio without including droplet. However, at the sub-channel outlet, the split droplets re-merge, as seen at t = 2.61 *ms*.

For an increased W_p to $0.75\,W_{ch}$, the droplet breakup is shown in Fig. 6. The continuous (primary) phase flowing through the sub-channel 2 is faster than the case of $W_p = 0.6\,W_{ch}$, and V_2 is 59%. After the split droplet exits the sub-channel, the droplets remain separated, as seen at t = 2.22 *ms*. However, at t = 2.76 *ms*, the stream of the

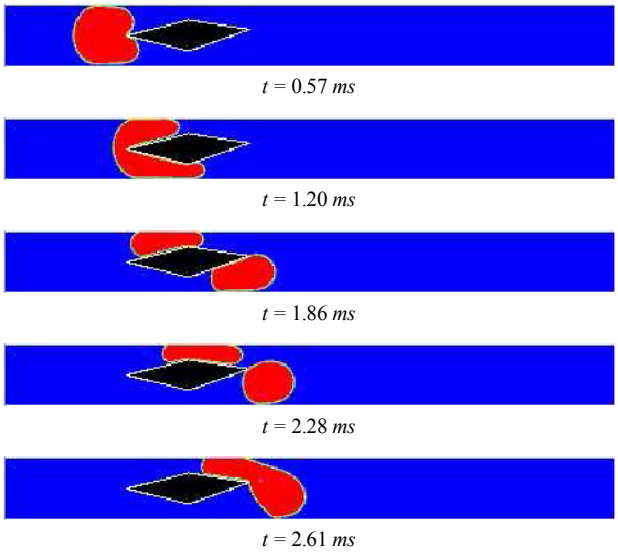

Fig. 4. Droplet breakup by a diamond-shape obstacle of $W_p = 0.6\,W_{ch}$.

Fig. 5. Steady-state velocity field without including a droplet for $W_p = 0.6\,W_{ch}$.

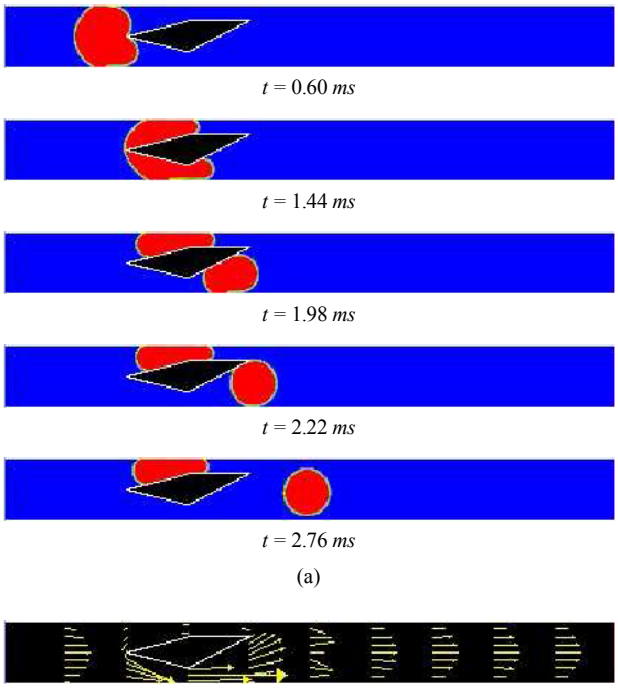

Fig. 6. Droplet breakup by a diamond-shape obstacle of $W_p = 0.75\,W_{ch}$: (a) droplet motion; (b) velocity field at $t = 2.76\ ms$.

continuous phase only moves through sub-channel 2 as depicted in Fig. 6(b). This result indicates that when W_p is large, the droplet can break up but the droplet flowing through the narrow sub-channel is stuck between the channel and the obstacle.

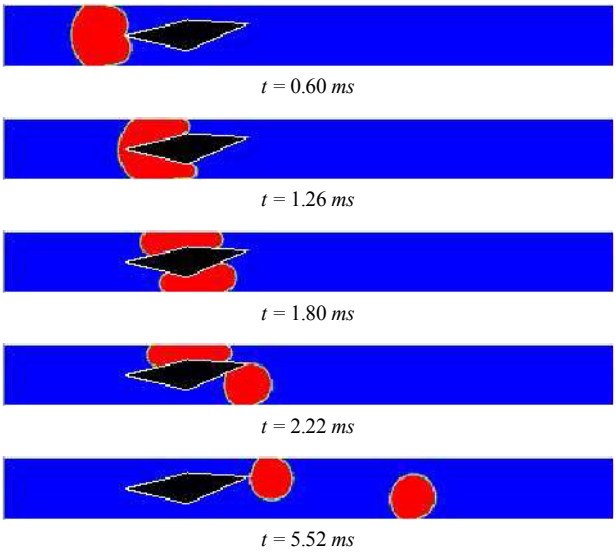

Fig. 7. Droplet breakup by a diamond-shape obstacle of $W_p = 0.69\,W_{ch}$.

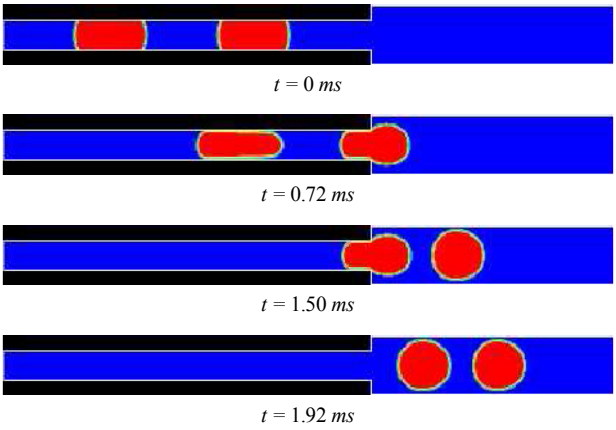

Fig. 8. Droplet merging by an enlarged chamber of $W_{cham} = 2\,W_{ch}$.

Fig. 7 describes the droplet breakup for $W_p = 0.69\,W_{ch}$. Two droplets show some distance after passing by the obstacle without the stagnation of the droplet. Also, V_2 is reduced to 56%. Among the three cases of diamond-shaped obstacle, the case of $W_p = 0.69\,W_{ch}$ is the most effective to split droplet without re-merging.

3.2 Droplet merging

The computational domain for droplet merging consists of three parts: inlet channel, enlarged chamber and outlet channel, as depicted in Fig. 1(b). As a method of droplet merging, the variation of channel geometry was tested with an enlarged chamber varying the width W_{cham} while keeping $L_{cham} = 0.3\ mm$, $W_{ch} = 36\ \mu m$ and $u_{in} = 0.2\ m/s$.

Fig. 8 shows the droplet merging at $W_{cham} = 2\,W_{ch}$. The velocity $U_{droplet}$ of droplet is obtained as $1.1\,u_{in}$ and the

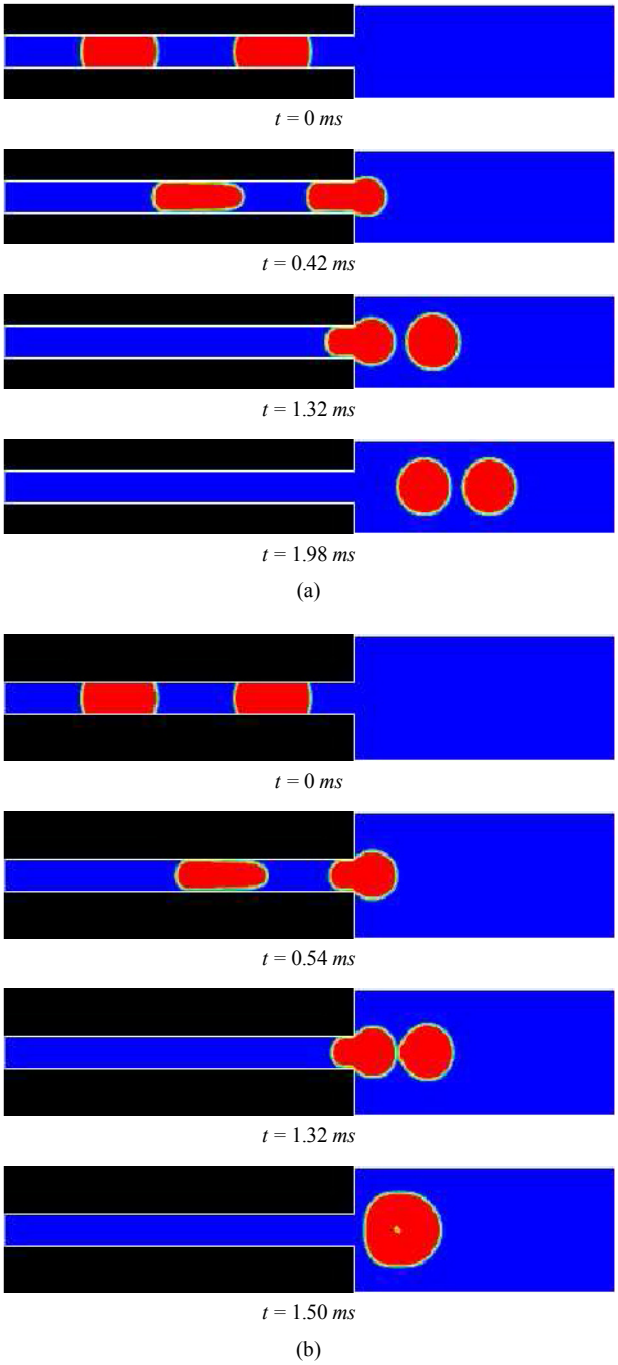

Fig. 9. Droplet merging by an enlarged chamber: (a) $W_{cham} = 3\,W_{ch}$; (b) $W_{cham} = 4\,W_{ch}$.

distance $D_{droplets}$ between two droplets is $4.8\,W_{ch}$ in the inlet channel. When the droplet enters the chamber, $U_{droplet}$ is decreased to $0.85\,u_{in}$ and the droplet becomes convex-shape by varying curvature as depicted in t = 0.72 *ms*. After two droplets enters the chamber, $U_{droplet}$ is $0.55\,u_{in}$ and $D_{droplets}$ is $2.8\,W_{ch}$.

For an increased W_{cham} to $3\,W_{ch}$, $U_{droplet}$ is decreased to $0.75\,u_{in}$ in the chamber. After the droplet enters the chamber, $U_{droplet}$ becomes $0.35\,u_{in}$ and $D_{droplets}$ is $2.1\,W_{ch}$ as presented in Fig. 9(a). When the chamber width is further increased to $4\,W_{ch}$, as depicted in Fig. 9(b), $U_{droplet}$ is obtained as $0.7\,u_{in}$ at the entrance of the chamber. After the droplet enters the chamber, $U_{droplet}$ is $0.2\,u_{in}$ and two droplets merge as shown in t = 1.50 *ms*. The results indicate that the condition of $W_{cham} \geq 4\,W_{ch}$ is required for droplet merging.

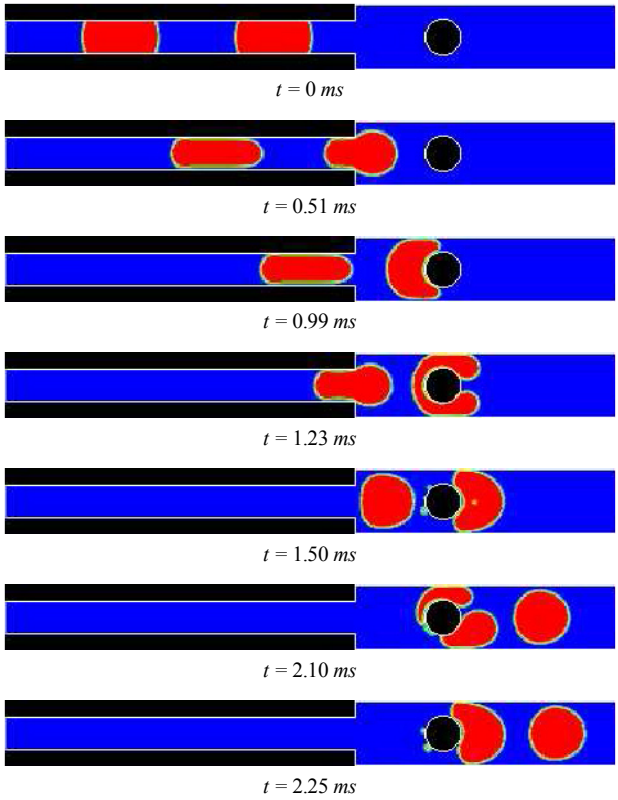

Fig. 10. Droplet merging by a circular obstacle of $\theta_{ob} = 175°$.

The use of an enlarged chamber is a popular method for droplet merging, but it requires a large space. Therefore, we tested another method of droplet merging without increasing the chamber width beyond $2\,W_{ch}$. The circular obstacle of $D_{ob} = 1.1\,W_{ch}$ is located at $x = 0.13\,L_{cham}$. We varied the contact angle θ_{ob} at the obstacle.

Fig. 10 shows droplet merging with an obstacle of θ_{ob} = 175°. While the first droplet passes around the obstacle, its velocity is not sufficiently reduced to merge with the next droplet. The droplet-droplet distance $D_{droplets}$ is obtained as $2.6\,W_{ch}$ in the chamber as shown at t = 1.50 *ms*.

For a decreased θ_{ob} to 30° as depicted in Fig. 11, the first droplet has sufficient time to merge with the second droplet because of the small contact angle as shown at t = 1.20 *ms*. Droplet merging occurs in the chamber as shown at t = 1.62 *ms*. However, when the merged droplet moves away from the obstacle, a small portion of the merged droplet is separated and remains at the obstacle as shown at t = 3.42 *ms*.

In the case of $\theta_{ob} = 60°$ depicted in Fig. 12, the small portion of droplet separated from the merged droplet does not

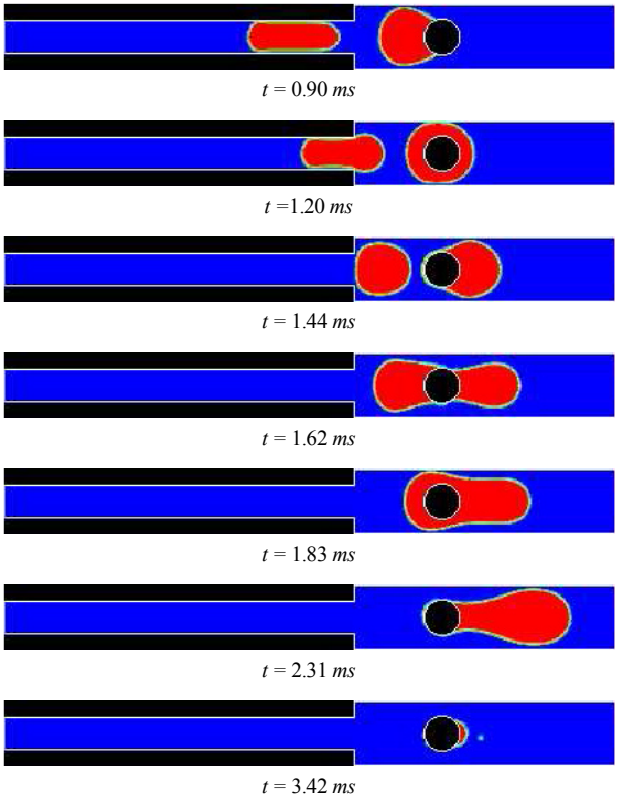

Fig. 11. Droplet merging by a circular obstacle of $\theta_{ob} = 30^\circ$.

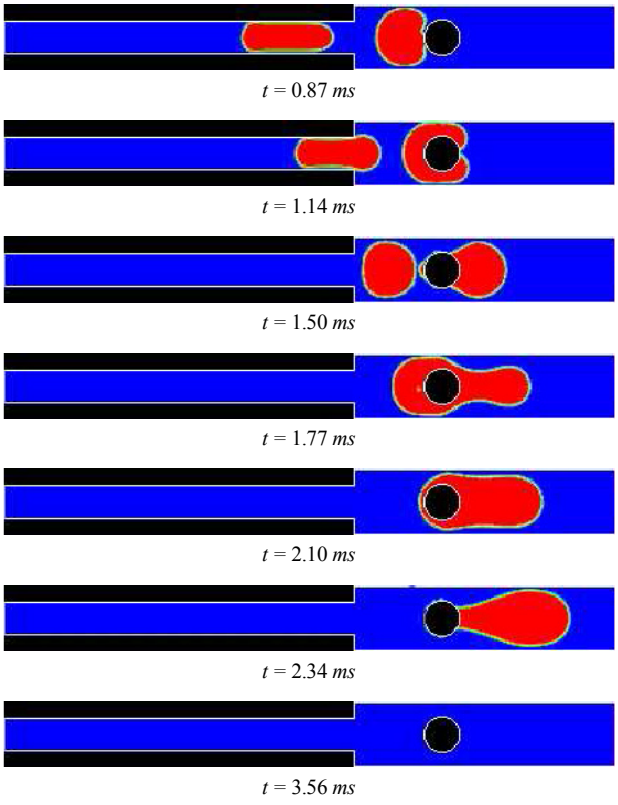

Fig. 12. Droplet merging by a circular obstacle of $\theta_{ob} = 60^\circ$.

appear as depicted at $t = 3.56\,ms$. This means that the optimal contact angle exists for droplet merging. Among the three cases of droplet merging with a circular obstacle, the case of $\theta_{ob} = 60^\circ$ is the most effective for droplet merging.

4. Conclusions

Droplet breakup and merging in a microchannel were investigated numerically by using the VOF method of the commercial code FLUENT. The numerical simulations of droplet breakup showed that the diamond-shaped obstacle is effective for droplet breakup, and the sub-channel width W_p at the obstacle end is one of the important parameters to determine the droplet breakup pattern. The split droplets re-merge at $W_p = 0.6\,W_{ch}$ and the split droplet is stuck in the narrow sub-channel at $W_p = 0.75\,W_{ch}$. The condition of $W_p = 0.69\,W_{ch}$ is the optimum for droplet breakup without re-merging and the split droplets have almost equal volumes.

The numerical simulations of droplet merging demonstrated that an obstacle can be used to significantly reduce the required chamber size. Droplet merging without an obstacle requires the chamber width larger than $4\,W_{ch}$. The use of a circular obstacle reduces the required chamber width to $2\,W_{ch}$. The contact angle of obstacle affects the droplet merging pattern. The contact angle of 60° is the optimum condition for droplet merging without re-splitting.

Acknowledgment

This work was supported by the National Research Foundation of Korea (NRF) grant No. 20090083510 funded by the Korean government (MEST) through Multi-phenomena CFD Engineering Research Center.

Nomenclature

$D_{droplet}$	: Distance between droplets
D_{ob}	: Diameter of obstacle
h	: Grid spacing
L_{ch}	: Length of channel
L_{cham}	: Length of chamber
L_{ob}	: Length of obstacle
Q_1	: Volume flow rate in sub channel 1
Q_2	: Volume flow rate in sub channel 2
$\boldsymbol{u}$	: Flow velocity vector, (u,v)
$U_{droplet}$	: Velocity of droplet
u_{in}	: Initial velocity
V_1	: Volume of droplet in sub-channel 1
V_2	: Volume of droplet in sub-channel 2
W_{ch}	: Width of channel
W_{cham}	: Width of chamber
W_{ob}	: Width of obstacle
W_p	: Width of sub-channel 2 at the obstacle end
W_1	: Width of sub-channel 1
W_2	: Width of sub-channel 2
θ_{ob}	: Contact angle of obstacle

κ : Interface curvature
σ : Surface tension coefficient

References

[1] S. Y. Teh, R. Lin, L. H. Hung and A. P. Lee, Droplet microfluidics, *Lab Chip*, 13 (2) (2008) 198-220.

[2] R. Seemann, M. Brinkmann, T. Pfohi and S. Herminghaus, Droplet based microfluidics, *Reports on progress in physics*, 75 (1) (2012) 016601.

[3] B. Kintses, L. D. Vliet, S. R. Devenish and F. Hollfelder, Microfluidic droplets: new integrated workflows for biological experiments, *Current opinion in chemical boilogy*, 14 (5) (2010) 548-555.

[4] S. Jayaraj, S. Kang and Y. K. Suh, A review on the analysis and experiment of fluid flow and mixing in micro-channels, *J. Mech. Sci. Technol.*, 21 (3) (2007) 536-548.

[5] H. Song, M. R. Bringer, J. D. Tice, C. J. Gerdts and R. F. Ismagilov, Experimental test of scaling of mixing by chaotic advection in droplets moving through microfluidic channels, *Appl. Phy. Lett* (83) (2003) 4464-4666.

[6] D. R. Link, S. L. Anna, D. A. Weitz and H. A. Stone, Geometrically mediated breakup of drops in microfluidic devices, *Appl. Phy. Lett* (92) (2004) 54503-1-4.

[7] K. Liu, H. Ding, Y. Chen and X. Zhao, Droplet-based synthetic method using microflow focusing and droplet fusion, *Microfluid. Nanofluid* (3) (2007) 239-243.

[8] Y. C. Tan, Y. L. Ho and A. P. Lee, Droplet coalescence by geometrically mediated flow in microfluidic channels, *Microfluid. Nanofluid* (3) (2007) 495-499.

[9] J. M. Kohler, Th. Henkel, A. Grodrian, Th. Kirner, M. Roth, K. Martin and J. Metze, Digital reaction technology by micro segmented flow—components, concepts and applications, *Chem. Eng. J* (101) (2004) 201-216.

[10] V. Chokkalingam, B. Weindenhof, M. Kramer, W. F. Maier, S. Herminghaus and R. Seemann, Optimized droplet-based microfluidics scheme for sol–gel reactions, *Lab Chip* (10) (2010) 1700-1705.

[11] D. E. Menech, Modeling of droplet breakup in a microfluidic T-shaped junction with a phase-field model, *Phys. Rev. E* (73) (2006) 031505.

[12] A. Carlson, M. Do-Quang and G. Amberg, Droplet dynamics in a bifurcating channel, *Int. J. Multiphase Flow* (36) (2010) 397-405.

[13] C. Chung, M. Lee, K. A. Char and K. H. Ahn, S. J. Lee, Droplet dynamics passing through obstructions in confined microchannel flow, *Microfluid. Nanofluid* (9) (2010) 1151-1163.

[14] M. Kadoura, Numerical analysis of sessile drop flow for electrowetting-on-dielectric devices, *Univ. Toronto* (2008) 1-55.

Gihun Son received his B.S. and M.S. degrees in Mechanical Engineering from Seoul National University in 1986 and 1988, respectively, and his Ph.D. in Mechanical Engineering from UCLA in 1996. Dr. Son is currently a professor of Mechanical Engineering at Sogang University in Seoul, Korea. His research interests are in the areas of multiphase dynamics, heat transfer, and power system simulation.

Jaewon Lee received a B.S. degree in Mechanical Engineering from Sogang University in 2013. He is a graduate student of Mechanical Engineering at Sogang University in Seoul, Korea. Mr. Lee's research interests are in the area of microfluidics and multiphase dynamics.